Journal of Advanced Research (2013) 4, 137–145

Cairo University

Journal of Advanced Research

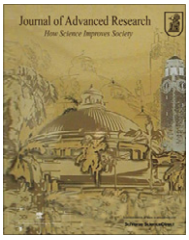

ORIGINAL ARTICLE

# Semi-empirical correlation for binary interaction parameters of the Peng–Robinson equation of state with the van der Waals mixing rules for the prediction of high-pressure vapor–liquid equilibrium

**Seif-Eddeen K. Fateen *, Menna M. Khalil, Ahmed O. Elnabawy**

*Department of Chemical Engineering, Faculty of Engineering, Cairo University, P.O. Box 12613, Giza, Egypt*

Received 13 December 2011; revised 29 March 2012; accepted 29 March 2012
Available online 5 May 2012

**KEYWORDS**

Peng–Robinson equation of state;
Vapor–liquid equilibrium;
Mixing rules;
Binary interaction parameters

**Abstract** Peng–Robinson equation of state is widely used with the classical van der Waals mixing rules to predict vapor liquid equilibria for systems containing hydrocarbons and related compounds. This model requires good values of the binary interaction parameter $k_{ij}$. In this work, we developed a semi-empirical correlation for $k_{ij}$ partly based on the Huron–Vidal mixing rules. We obtained values for the adjustable parameters of the developed formula for over 60 binary systems and over 10 categories of components. The predictions of the new equation system were slightly better than the constant-$k_{ij}$ model in most cases, except for 10 systems whose predictions were considerably improved with the new correlation.



## Introduction

The use of simple equations of state for the calculations of Vapor–Liquid Equilibrium (VLE) is preferred by practicing engineers over the use of more complicated models [1]. Cubic equations of state have gained overwhelming acceptance as a robust and reliable, yet relatively simple, model for predicting VLE of high-pressure systems. Mixing rules are used in conjunction with cubic equations of state for the complete representations of fluid mixtures. These mixing rules require empirically-determined Binary Interaction Parameters (BIPs) to describe the VLE more accurately. The lack of those binary interaction parameters often result in inaccurate VLE predictions.

* Corresponding author. Tel.: +20 111 400 8888; fax: +20 202 3749 7646.
E-mail addresses: fateen@eng1.cu.edu.eg, sfateen@alum.mit.edu (S.-E.K. Fateen).

Peer review under responsibility of Cairo University.

ELSEVIER Production and hosting by Elsevier

2090-1232 © 2012 Cairo University. Production and hosting by Elsevier B.V. All rights reserved.
http://dx.doi.org/10.1016/j.jare.2012.03.004

**Nomenclature**

| | |
|---|---|
| $A$ | equation of state parameter |
| $b$ | equation of state parameter |
| K | Kelvin |
| $k_{ij}$ | binary interaction parameters, dimensionless |
| OF | objective function |
| $P$ | absolute pressure, bar |
| Pxy | a phase diagram that has pressure on its $y$-axis and both the liquid composition ($x$) and the vapor composition ($y$) on its $x$-axis. |
| $R$ | Universal gas constant, 8.314 $m^3$ Pa/K mole |
| RMSE | Root Mean Square Error |
| $T$ | absolute temperature, K |
| $V$ | molar volume, $m^3$/mole |
| $x$ | liquid phase mole fraction |
| $x_i$ | liquid phase mole fraction of $i$th component |
| $y$ | vapor phase mole fraction |
| $Z$ | compressibility factor |

*Greek letters*

| | |
|---|---|
| $\hat{\varphi}_i$ | fugacity coefficient of $i$th component |
| $\gamma_i$ | activity coefficient of $i$th component |
| $\theta_1$, $\theta_2$, $\theta_3$ | adjustable parameters, dimensionless |

*Superscript*

| | |
|---|---|
| $E$ | excess property |
| $\infty$ | at infinite pressure |
| $V$ | vapor phase property |
| $L$ | liquid phase property |

The experimental data needed for the generation of BIPs may be difficult or too costly to obtain. Thus, the development of simple models for the prediction of high-pressure VLE with no need for experimental data is an important research objective. Several successful attempts have been made to introduce an equation system based on the combination of a cubic equation of state with appropriate mixing rules to predict the VLE without the need of binary interaction parameters fitted from experimental data.

Peng–Robinson [2] (PR) equation of state is one of the most popular cubic equations of state. It has been used extensively in process simulation tools to model the high-pressure VLE behavior. Among the commonly used mixing rules are Huron–Vidal [3] and Wong–Sandler [4]. Other mixing rules have been successfully used. A review on the available mixing rules is available elsewhere [5].

The objective of this work is to provide good estimates for binary interaction parameters to be used with the simplest and most widely-used equations system for the prediction of high-pressure vapor–liquid equilibrium. Thus, we estimate generalized values of the binary interaction parameters to be used with Peng–Robinson equation of state combined with van der Waals mixing rules. The work was limited to systems of hydrocarbons and related compounds.

The novelty of this work lies in the development of a general correlation for the binary interaction parameter of van der Waals mixing rules and the generation of the values of the adjustable parameters of the developed correlation that can be used to predict, with good accuracy, the vapor–liquid equilibrium of the studied systems.

The remainder of this paper is organized as follows. The next section introduces the Huron–Vidal and the van der Waals mixing rules as applied to the Peng–Robinson equation of state. The following section introduces the semi-empirical correlation that is developed in this work. Next, the methodology used to fit the experimental data and verify the correlation is presented. The following section presents the results of the work, discusses its significance and gives examples of the application of the newly-developed correlation to ternary systems. The last section ends with this work's conclusions.

## Huron–Vidal and van der Waals mixing rules for the Peng–Robinson equation of state

In this and the following section, we present the theoretical basis for the proposed semi-empirical correlation. The thermodynamic properties and concepts used in this analysis follow the framework used in Orbey and Sandler [5]. The Peng–Robinson equation of state

$$P = \frac{RT}{V-b} - \frac{a}{V(V+b)+b(V-b)} \tag{1}$$

can be used with the van der Waals mixing rules,

$$a = \sum_i \sum_j z_i z_j \sqrt{a_i a_j}(1-k_{ij}) \tag{2}$$

$$b = \sum_i x_i b_i \tag{3}$$

to predict the vapor–liquid equilibrium via the calculation of the fugacity coefficient of the liquid and the vapor phases according to

$$\ln\hat{\varphi}_i = \frac{b_i}{b}(Z-1) - \ln(Z-B) - \frac{A}{2\sqrt{2}B}\left(\frac{2\sum_j z_j a_{ij}}{a} - \frac{b_i}{b}\right)\ln\left[\frac{Z+(1+\sqrt{2})B}{Z+(1-\sqrt{2})B}\right] \tag{4}$$

where $B = bP/RT$, $A = aP/(RT)^2$, and $Z = PV/RT$. The fugacity coefficient is a measure of the deviation from the ideal-gas mixture behavior and is used in the phase equilibrium equation. The Huron–Vidal mixing rules use a different equation for the $a$ parameter as follows:

$$a = b\left[\sum_i z_i \frac{a_i}{b_i} + \frac{G^{ex}_{\gamma}}{C^*}\right], \tag{5}$$

where $C^* = -0.62323$ for the Peng–Robinson equation of state. The resulting fugacity coefficient equation when using Huron–Vidal mixing rules becomes

$$\ln\hat{\varphi}_i = \frac{b_i}{b}(Z-1) - \ln(Z-B) - \frac{1}{2\sqrt{2}}\left(\frac{a_i}{b_i RT} + \frac{\ln\gamma_i}{C^*}\right)\ln\left[\frac{Z+(1+\sqrt{2})B}{Z+(1-\sqrt{2})B}\right] \quad (6)$$

### Semi-empirical correlation for the binary interaction parameter

Soave and Gamba [6] showed that the van der Waals mixing rules correspond to a special case of the Huron–Vidal mixing rules, when the regular solution description is used to express excess Gibbs at infinite pressure. Excess Gibbs is the difference between Gibbs energy of a mixture and Gibbs energy of an ideal mixture at the same conditions. The equivalency of the two fugacity coefficient equations (Eqs. (4) and (6)) can be used to relate the van der Waals binary interaction parameter, $k_{ij}$, to the activity coefficient, which accounts for the deviations from ideal behavior of the mixture.

$$\frac{a_i}{b_i RT} + \frac{\ln\gamma_i}{C^*} = \frac{a}{bRT}\left(\frac{2\sum_j z_j a_{kj}}{a} - \frac{b_i}{b}\right) \quad (7)$$

To remove the composition dependence of the activity coefficient, we consider the particular case of component 1 at infinite dilution in component 2 following the derivation of Soave and Gamba [6]. Thus, Eq. (7) becomes

$$\frac{a_1}{b_1 RT} + \frac{\ln\gamma_1^\infty}{C^*} = \frac{a_2}{b_2 RT}\left(2\sqrt{\frac{a_1}{a_2}}(1-k_{12}) - \frac{b_1}{b_2}\right) \quad (8)$$

Solving for the binary interaction parameter, $k_{12}$, we get

$$k_{12} = 1 - \frac{1}{2}\frac{b_2}{b_1}\sqrt{\frac{a_1}{a_2}} - \frac{1}{2}\frac{b_1}{b_2}\sqrt{\frac{a_2}{a_1}} - \frac{1}{2}\frac{b_2 RT}{C^*\sqrt{a_1 a_2}}\ln\gamma_1^\infty \quad (9)$$

The activity coefficient can be predicted using a predictive excess Gibbs model such as UNIFAC. For this case, the infinite-dilution activity coefficient can be used instead of the general composition-dependent activity coefficient. A simple way to predict the infinite-dilution activity coefficient is to use the Scatchard–Hildebrand equations [7] for regular solutions, which provides an expression for the infinite-dilution activity coefficient when the liquid volumes are replaced by the co-volumes $b$. The infinite-dilution activity coefficient at infinite pressure becomes

$$\ln\gamma_1^\infty = -\frac{b_1 C^*}{2RT}\left(\frac{a_1}{b_1^2} + \frac{a_2}{b_2^2} - \frac{2a_{12}}{b_1 b_2}\right). \quad (10)$$

Instead of using Eq. (10) for the infinite-dilution activity coefficient at infinite pressure, we replace it with a simple empirical correlation that takes into account the effect of temperature. The correlation also accounts for the effect of pressure. The target is to obtain a correlation for the binary interaction parameter that can fit the experimental data with a minimum set of parameters and can be used for similar systems, for which no experimental data is available. Hence, the dependence on pressure will deem this correlation more versatile and useful. The empirical correlation used is

$$\ln\gamma_1^\infty = -C^*\frac{\theta_1}{T_{r_1}^{\theta_2} P_{r_1}^{\theta_3}}, \quad (11)$$

where $\theta_1$, $\theta_2$ and $\theta_3$ are adjustable parameters. The final correlation for the binary interaction parameter becomes

$$k_{12} = 1 - \frac{1}{2}\frac{b_2}{b_1}\sqrt{\frac{a_1}{a_2}} - \frac{1}{2}\frac{b_1}{b_2}\sqrt{\frac{a_2}{a_1}} + \frac{1}{2}\frac{b_2 RT}{\sqrt{a_1 a_2}}\frac{\theta_1}{T_{r_1}^{\theta_2} P_{r_1}^{\theta_3}}. \quad (12)$$

Note that the above equation allows for unsymmetrical binary interaction parameters, which may be tempting to pursue. The same formula can be used to calculate a different $k_{21}$ when the reduced temperature and pressure for the second components are used. However, the use of unsymmetrical binary interaction parameters proved to result in unrealistic prediction of the phase behavior close to the critical point. Thus in this work, $k_{12} = k_{21}$ was used in the calculations.

Since the resulting correlations contain details about the two components in the system as well as the temperature and pressure, it was expected that the adjustable parameters for similar substances would be similar. The values of the adjustable parameters were obtained for hydrocarbon systems and related compounds. Similar categories of substances were identified and adjustable parameters for those categories were also obtained. These parameters can be reused with similar systems for which no experimental data are available.

### Experimental data fitting

Data for hydrocarbon systems and related compounds were obtained from a variety of literature sources [8–51]. The first column in Table 1 enumerates the systems considered. The second column gives their names. The third and the fourth columns give the number of data sets and the number of data points, respectively.

For comparison, values for the constant binary interaction parameter for the Peng–Robinson equation of state with the classical van der Waals mixing rules were obtained from the database of the AspenPlus software and used to give predictions of the equilibrium at the temperatures of all data sets.

The three adjustable parameters for the binary interaction parameter $k_{ij}$ were adjusted to fit the experimental data for each of the systems mentioned in Table 1. Bubble point calculations were performed at every experimental liquid composition to calculate the bubble pressure and the vapor composition. The bubble point calculations estimate the pressure at which the first bubble of vapor is formed when reducing the pressure of a liquid mixture and they also estimate the composition of the first bubble formed.

The algorithm for the bubble point calculations at each point consisted of two loops; the function of the inner loop was to change the vapor mole fraction to satisfy the equilibrium relation between the vapor composition and the liquid composition

$$y_i = \frac{\hat{\varphi}_i^L}{\hat{\varphi}_i^V} x_i \quad (13)$$

Broyden's method [52] was used to facilitate the conversion of the inner loop. The function of the outer loop was to change the pressure to satisfy the summation of the vapor mole fraction equation $\sum_i y_i = 1$. A phase stability check was performed according to Michelsen's method [53] for the obtained bubble pressure to ensure that it satisfies the two-phase condition.

A minimum value of the deviation between the experimental points and the model prediction was sought by adjusting the three adjustable parameters to minimize the following objective function:

**Table 1** Experimental data sets used in this study, the values of the adjustable parameters, the RMSE of the regression using the developed formula and the RMSE of the constant-$k$ approach.

| # | Component 1/component 2 | No. of sets | No. of points | $\theta_1$ | $\theta_2$ | $\theta_3$ | RMSE | $k_{12}$ | RMSE of const. $k_{12}$ |
|---|---|---|---|---|---|---|---|---|---|
| 1 | Benzene/heptane | 2 | 29 | 1.7793 | −22.8298 | 2.2481 | 0.0776 | 0.0011 | 0.0947 |
| 2 | Carbon dioxide/benzene | 4 | 30 | 0.96606 | 0.37215 | 0.043118 | 0.0492 | 0.0774 | 0.107 |
| 3 | Carbon dioxide/decane | 9 | 91 | 1.483 | 1.5912 | 0.0600 | 0.0384 | 0.1141 | 0.0485 |
| 4 | Carbon dioxide/ethane | 15 | 208 | 1.4235 | −1.969 | 0.51141 | 0.0331 | 0.1322 | 0.0462 |
| 5 | Carbon dioxide/heptane | 4 | 63 | 1.4284 | 2.212 | −0.018053 | 0.0395 | 0.1 | 0.0478 |
| 6 | Carbon dioxide/i-butane | 7 | 95 | 1.1552 | −0.5271 | 0.040874 | 0.0552 | 0.12 | 0.0829 |
| 7 | Carbon dioxide/i-pentane | 7 | 75 | 1.004 | −0.61396 | 0.18009 | 0.0845 | 0.1219 | 0.128 |
| 8 | Carbon dioxide/m-xylene | 4 | 16 | 0.63027 | 0.018652 | 0.086257 | 0.0496 | 0.14339[a] | 0.0699 |
| 9 | Carbon dioxide/n-butane | 21 | 285 | 1.3967 | 1.1904 | 0.047138 | 0.0663 | 0.1333 | 0.0743 |
| 10 | Carbon dioxide/n-hexane | 7 | 75 | 1.3196 | 1.1245 | 0.079638 | 0.0260 | 0.11 | 0.0622 |
| 11 | Carbon dioxide/n-pentane | 17 | 190 | 1.308 | 0.72998 | 0.078627 | 0.0922 | 0.1222 | 0.109 |
| 12 | Carbon dioxide/octane | 5 | 39 | 1.3958 | 0.91696 | 0.10569 | 0.0277 | 0.13303[a] | 0.0496 |
| 13 | Carbon dioxide/propane | 20 | 306 | 1.4085 | 0.25463 | 0.073905 | 0.0426 | 0.1241 | 0.0576 |
| 14 | Carbon dioxide/toluene | 7 | 36 | 1.1807 | 1.4945 | 0.084523 | 0.0623 | 0.1056 | 0.0777 |
| 15 | Ethane/benzene | 1 | 7 | 0.5452 | 7.3061 | 0.2326 | 0.0210 | 0.0322 | 0.0749 |
| 16 | Ethane/heptane | 5 | 32 | 0.0848 | −0.1268 | −2.6938 | 0.0342 | 0.0067 | 0.0421 |
| 17 | Ethane/hexane | 4 | 48 | 0.3191 | −0.1129 | −2.5086 | 0.134 | −0.01 | 0.146 |
| 18 | Ethane/hydrogen sulfide | 4 | 45 | 2.4607 | 0.80676 | −0.062934 | 0.0581 | 0.0833 | 0.166 |
| 19 | Ethane/i-butane | 4 | 40 | 0.071971 | −4.9954 | 0.86325 | 0.105 | −0.0067 | 0.121 |
| 20 | Ethane/n-butane | 7 | 62 | 0.3157 | 0.2182 | −1.9626 | 0.122 | 0.0096 | 0.127 |
| 21 | Ethane/octane | 4 | 46 | 0.2874 | 0.4289 | −0.0239 | 0.0223 | 0.0185 | 0.0273 |
| 22 | Ethane/propane | 10 | 204 | 0.00182 | −0.89866 | −4.048 | 0.0477 | 0.0011 | 0.0467 |
| 23 | Hexane/benzene | 4 | 40 | 4.1217 | −22.6636 | 2.097 | 0.0581 | 0.0093 | 0.0701 |
| 24 | Hydrogen sulfide/benzene | 3 | 24 | 0.23964 | 0.68015 | −0.098572 | 0.0173 | 0.00293[a] | 0.0191 |
| 25 | Hydrogen sulfide/butane | 6 | 63 | 0.8006 | −2.5291 | 0.44581 | 0.0788 | 0.11554[a] | 0.0929 |
| 26 | Hydrogen sulfide/decane | 6 | 55 | 1.1815 | 1.2244 | 0.03983 | 0.0522 | 0.0333[a] | 0.0571 |
| 27 | Hydrogen sulfide/heptane | 7 | 69 | 1.2103 | 0.5664 | 0.059205 | 0.0637 | 0.06164[a] | 0.0755 |
| 28 | Hydrogen sulfide/hexane | 3 | 25 | 1.1128 | 1.4782 | 0.0254 | 0.0361 | 0.05744[a] | 0.0369 |
| 29 | Hydrogen sulfide/i-butane | 5 | 53 | 0.9219 | −3.5258 | 0.4963 | 0.0657 | 0.0474 | 0.110 |
| 30 | Hydrogen sulfide/m-xylene | 4 | 30 | 0.16833 | −0.7745 | 0.52783 | 0.0563 | 0.0172[a] | 0.104 |
| 31 | Hydrogen sulfide/pentane | 5 | 55 | 1.1753 | 0.59399 | 0.035541 | 0.0481 | 0.063 | 0.103 |
| 32 | Hydrogen sulfide/toluene | 4 | 27 | 0.12967 | −1.6078 | 0.49196 | 0.0393 | 0.00751[a] | 0.0601 |
| 33 | Methane/benzene | 1 | 9 | 1.3016 | 1.3863 | −0.0135 | 0.0771 | 0.0363 | 0.0809 |
| 34 | Methane/carbon dioxide | 12 | 110 | 2.5522 | 0.80726 | 0.081903 | 0.0383 | 0.0919 | 0.0667 |
| 35 | Methane/ethane | 24 | 247 | 0.25631 | 1.0856 | −0.22141 | 0.0236 | −0.0026 | 0.0300 |
| 36 | Methane/heptane | 6 | 69 | 0.63543 | 2.6528 | 0.27181 | 0.0630 | 0.0352 | 0.105 |
| 37 | Methane/hexane | 16 | 164 | 0.47074 | 1.2722 | 0.12573 | 0.0699 | 0.0422 | 0.0935 |
| 38 | Methane/hydrogen sulfide | 6 | 87 | 2.1869 | 0.000377 | −0.0021896 | 0.0820 | 0.08857[a] | 0.106 |
| 39 | Methane/i-butane | 3 | 41 | 0.16027 | −0.88324 | 0.22258 | 0.03 | 0.0256 | 0.0487 |
| 40 | Methane/m-xylene | 1 | 11 | 1.3709 | 1.5864 | 0.020632 | 0.0433 | 0.0844 | 0.364 |
| 41 | Methane/n-butane | 18 | 174 | 0.26158 | 2.7064 | 0.007763 | 0.0359 | 0.0133 | 0.0412 |
| 42 | Methane/n-decane | 10 | 180 | 0.3349 | 0.66795 | −0.13221 | 0.0466 | 0.0422 | 0.0668 |
| 43 | Methane/nonane | 8 | 131 | 0.87786 | 2.0391 | 0.0062196 | 0.0317 | 0.0474 | 0.0715 |
| 44 | Methane/n-pentane | 20 | 192 | 0.38891 | 1.4822 | 0.10371 | 0.0530 | 0.023 | 0.0630 |
| 45 | Methane/propane | 16 | 283 | 0.21065 | −0.085365 | 0.16692 | 0.0429 | 0.014 | 0.0463 |
| 46 | Methane/toluene | 1 | 11 | 1.5806 | 1.3061 | 0.2421 | 0.0456 | 0.097 | 0.549 |
| 47 | Nitrogen/benzene | 3 | 15 | 10.9661 | 1.7329 | 0.054387 | 0.0203 | 0.1641 | 0.0659 |
| 48 | Nitrogen/butane | 7 | 94 | 4.5148 | 1.989 | 0.033379 | 0.103 | 0.08 | 0.117 |
| 49 | Nitrogen/carbon dioxide | 9 | 126 | 2.9856 | 0.7253 | 0.1121 | 0.0571 | −0.017 | 0.0851 |
| 50 | Nitrogen/ethane | 8 | 92 | 1.8177 | 1.1792 | 0.1195 | 0.0621 | 0.0515 | 0.133 |
| 51 | Nitrogen/heptane | 10 | 146 | 4.4672 | 1.2858 | 0.33427 | 0.116 | 0.1441 | 0.179 |
| 52 | Nitrogen/hexane | 7 | 79 | 6.8492 | 2.0403 | 0.1039 | 0.128 | 0.1496 | 0.145 |
| 53 | Nitrogen/hydrogen sulfide | 7 | 75 | 10.5967 | 1.4144 | −0.049292 | 0.131 | 0.1767 | 0.184 |
| 54 | Nitrogen/methane | 12 | 129 | 0.86611 | 0.43608 | −0.008506 | 0.0214 | 0.0311 | 0.0311 |
| 55 | Nitrogen/octane | 5 | 78 | 6.7118 | 1.6856 | 0.26848 | 0.102 | −0.41 | 0.474 |
| 56 | Nitrogen/pentane | 13 | 118 | 2.0432 | 0.98778 | 0.15599 | 0.103 | 0.1 | 0.120 |
| 57 | Nitrogen/propane | 3 | 32 | 2.0255 | 0.9579 | 0.11162 | 0.0272 | 0.0852 | 0.0479 |
| 58 | Nitrogen/toluene | 1 | 10 | 5.8773 | 1.2396 | 0.034697 | 0.0405 | 0.20142[a] | 0.0569 |
| 59 | Pentane/toluene | 5 | 55 | 0.12736 | −2.3266 | 0.5283 | 0.0275 | 0.00845[a] | 0.0335 |
| 60 | Propane/i-butane | 4 | 40 | −0.20668 | 3.8567 | −0.9207 | 0.0364 | −0.0078 | 0.0377 |
| 61 | Propane/i-pentane | 8 | 92 | 0.45184 | 3.8993 | −0.89997 | 0.0435 | 0.0111 | 0.0487 |

[a] $k_{ij}$ was not available in the Aspen database. Fitting was performed on the available data.

**Table 2** Categorization of the tested systems based on the RMSE difference between the result of the developed formula as opposed to the result of a constant binary interaction parameter.

| Difference in RMSE < 5% | Difference in RMSE between 5% and 10% | Difference in RMSE > 10% |
|---|---|---|
| All other tested systems not listed here | Nitrogen/ethane<br>Nitrogen/heptane<br>Carbon dioxide/benzene<br>Hydrogen sulfide/pentane<br>Ethane/benzene<br>Nitrogen/hydrogen sulfide | Methane/toluene<br>Nitrogen/octane<br>Methane/m-xylene<br>Ethane/hydrogen sulfide |

**Table 3** The values of the adjustable parameters for categories of systems and the respective RMSE.

| # | Category 1/category 2 | No. of sets | No. of points | $\theta_1$ | $\theta_2$ | $\theta_3$ | RMSE |
|---|---|---|---|---|---|---|---|
| 1 | Alkanes/alkanes | 46 | 591 | 0.22806 | 0.18772 | −0.96388 | 0.0661 |
| 2 | Alkanes/aromatics | 12 | 131 | 0.82592 | 9.78e−5 | −0.020973 | 0.0787 |
| 3 | Methane/light alkanes | 43 | 476 | 0.28737 | 1.626 | 0.064303 | 0.0529 |
| 4 | Carbon dioxide/light alkanes | 79 | 1046 | 1.413 | 1. 2593 | 0.047519 | 0.0657 |
| 5 | Carbon dioxide/heavy alkanes | 18 | 193 | 1.4656 | 1.707 | −0.009157 | 0.0537 |
| 6 | Carbon dioxide/aromatics | 15 | 82 | 1.0531 | 0.97216 | 0.049409 | 0.0632 |
| 7 | Hydrogen sulfide/heavy alkanes | 13 | 124 | 1.1677 | 0.89869 | 0.061973 | 0.0614 |
| 8 | Methane/heavy alkanes | 22 | 355 | 0.50209 | 0.99478 | 0.0087438 | 0.0645 |
| 9 | Methane/light alkanes | 87 | 1040 | 0.32192 | 0.82836 | 0.036413 | 0.0609 |
| 10 | Nitrogen/aromatics | 5 | 35 | 4.0915 | 0.86053 | 0.036825 | 0.0615 |
| 11 | Hydrogen sulfide/aromatics | 11 | 81 | 0.0967 | −1.7173 | 0.6559 | 0.0543 |

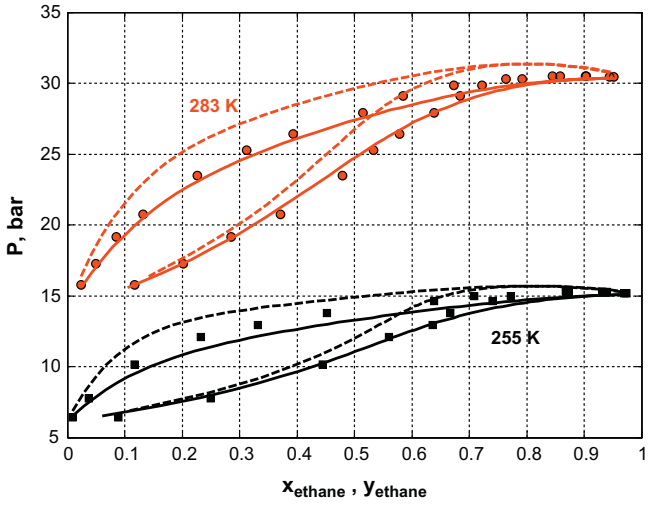


**Fig. 1** Pxy equilibrium diagram for ethane and hydrogen sulfide at 255 and 283 K using the semi-empirical correlation for $k_{ij}$ (solid line) ($\theta$ = [2.4607 0.80676 −0.06293]) as compared with the results of the constant-$k_{ij}$ calculations (dotted line) ($k_{ij}$ = 0.0833) and with published experimental data (markers) [56]. The pressure data points are within 0.1 bar.

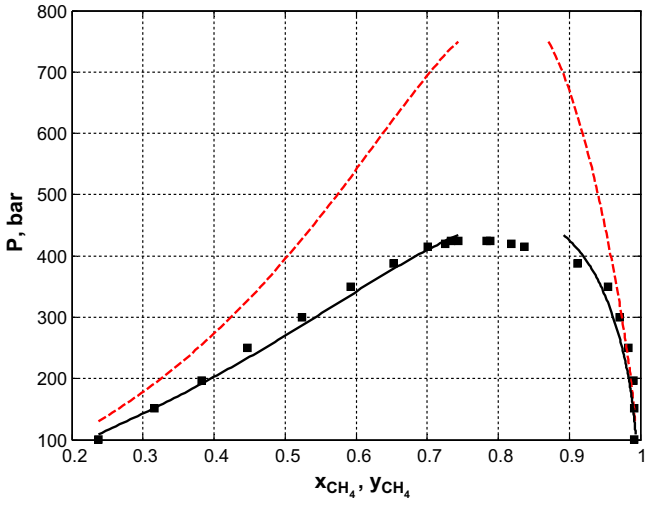


**Fig. 2** Pxy equilibrium diagram for methane and toluene at 313 K using the semi-empirical correlation for $k_{ij}$ (black solid line) ($\theta$ = [1.5806 1.3061 0.2421]) as compared with the results of the constant-$k_{ij}$ calculations (red dotted line) ($k_{ij}$ = 0.097) and with published experimental data (markers) [57]. The pressure data points are within 1 bar.

$$\mathrm{OF} = \sum_{is}\sum_{ip}\left[\left(1-\frac{P_{PR,ip,is}}{P_{\exp,ip,is}}\right)^2+\left(1-\frac{y_{PR,ip,is}}{y_{\exp,ip,is}}\right)^2\right] \tag{14}$$

where *is* is the index for the experimental data sets and *ip* is the index for the data points in each data set. In the data fitting procedure, this selected objective function equates the weight of the errors in the prediction of the pressure and the errors in the prediction of the vapor mole fraction so that the predictions would match both the experimental pressure and the experimental vapor composition as close as possible.

Minimization was performed using the MATLAB function fmincon, which attempts constrained nonlinear optimization.

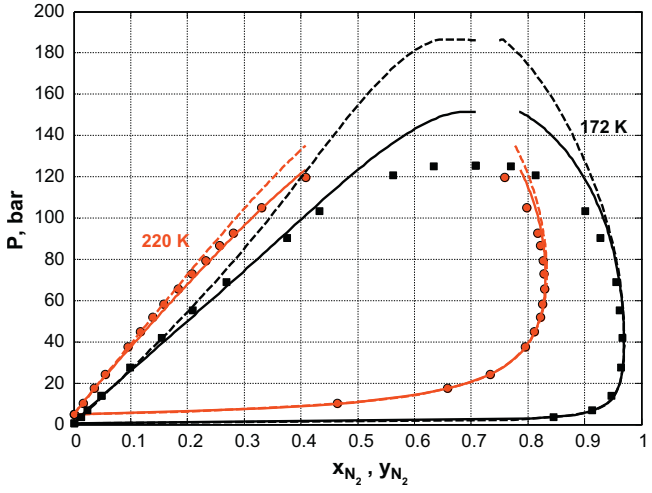


**Fig. 3** Pxy equilibrium diagram for nitrogen and ethane at 172 and 220 K using the semi-empirical correlation for $k_{ij}$ (solid line) ($\theta$ = [1.8177 1.1792 0.1195]) as compared with the results of the constant-$k_{ij}$ calculations (dotted line) ($k_{ij}$ = 0.0515) and with published experimental data (markers) [55,58].

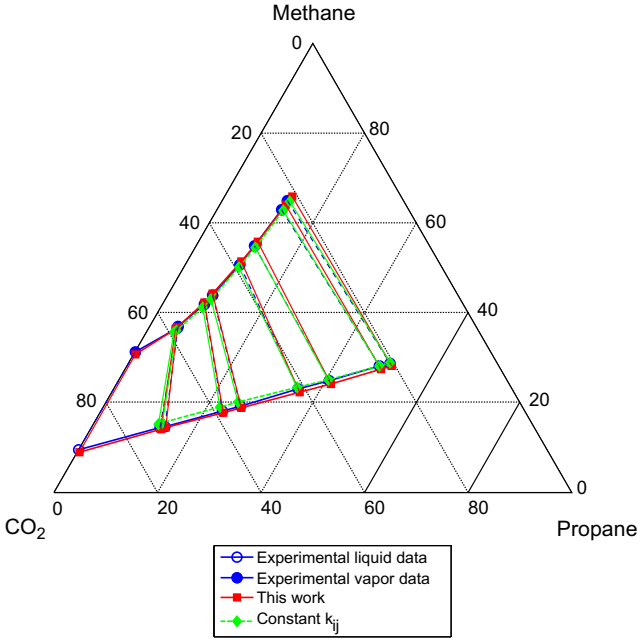


**Fig. 5** Ternary liquid vapor equilibrium diagram for methane, carbon dioxide and propane at 270 K and 55 bar using the semi-empirical correlation for $k_{ij}$ as compared with the results of the constant-$k_{ij}$ calculations and with published experimental data [54]. The scale of axes is in mole %.

The algorithm used with the minimization function was the interior-point algorithm. The iterations for minimization stopped when the relative change in all the adjustable parameters were less than $10^{-10}$. The initial point was usually taken as [0 1 1] for the adjustable-parameters vector. In some cases, the initial value caused convergence problems for the bubble point algorithm. In those cases, minimization was performed on a subset of the experimental data. Once those data points were fitted, the calculated values of the adjustable parameters were used as the initial point for a larger subset of the experimental data. This procedure was repeated until all the experimental data were included in the data fitting procedure.

An easier application of the developed formula would be to use lumped values for the adjustable parameters for categories of components. The formula could lend itself to category-based application because it already contains information about the critical points of the components. Thus, an attempt was made to obtain lumped values for the adjustable parameters for different categories by fitting the data sets of the liquid–vapor equilibrium of similar components. The above procedure was repeated for entire categories with larger data sets.

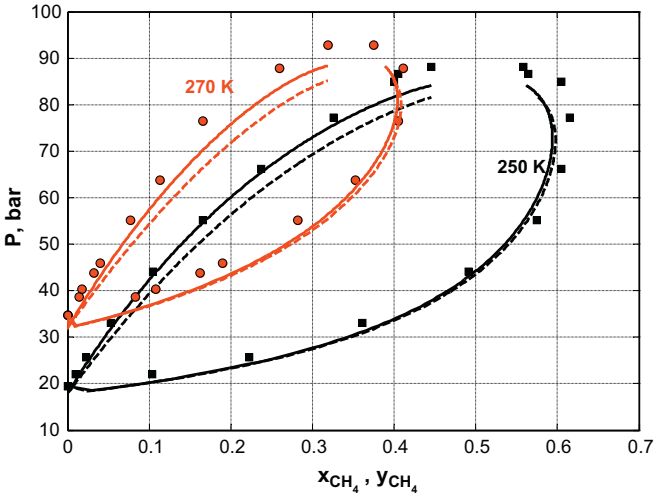


**Fig. 4** Pxy equilibrium diagram for methane and carbon dioxide at 250 and 270 K using the semi-empirical correlation for $k_{ij}$ (solid line) ($\theta$ = [2.5522 0.81726 0.0819]) as compared with the results of the constant-$k_{ij}$ calculations (dotted line) ($k_{ij}$ = 0.0919) and with published experimental data (markers) [58].

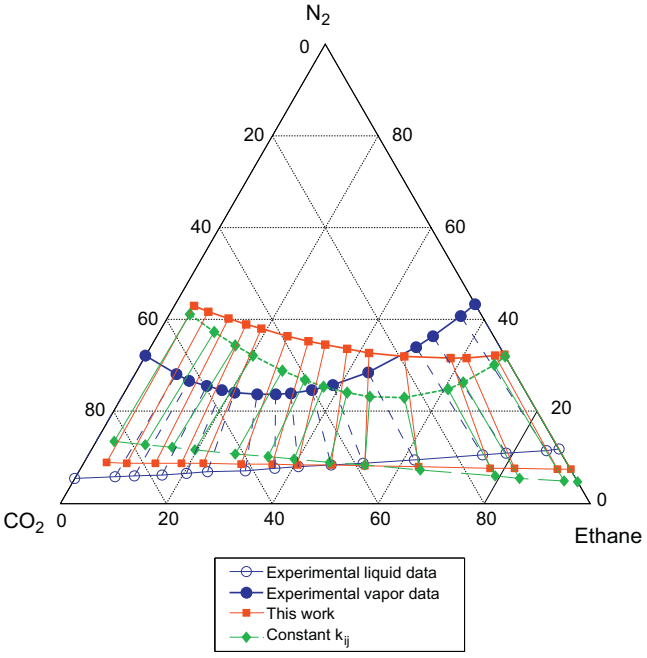


**Fig. 6** Ternary liquid vapor equilibrium diagram for nitrogen, carbon dioxide and ethane at 270 K and 60 bar using the semi-empirical correlation for $k_{ij}$ as compared with the results of the constant-$k_{ij}$ calculations and with published experimental data [55]. The blue line/markers represent the experimental data, the red lines/markers represent the results of this work and the green lines/markers represent the results of the constant-$k_{ij}$ calculations.

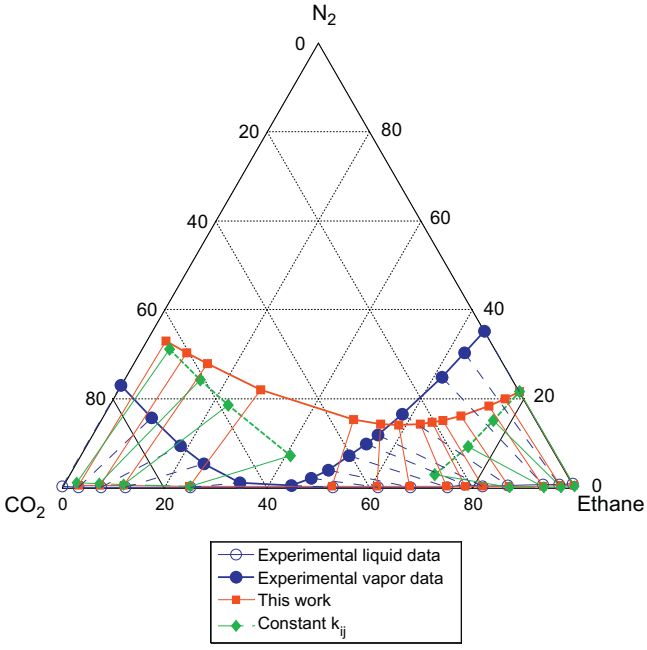


**Fig. 7** Ternary liquid vapor equilibrium diagram for nitrogen, carbon dioxide and ethane at 220 K and 8 bar using the semi-empirical correlation for $k_{ij}$ as compared with the results of the constant-$k_{ij}$ calculations and with published experimental data [55]. The blue line/markers represent the experimental data, the red lines/markers represent the results of this work and the green lines/markers represent the results of the constant-$k_{ij}$ calculations.

## Results and discussion

Table 1 shows the values obtained for the three adjustable parameters for each of the system considered. The Root Mean Square Error (RMSE), which is a measure of the differences between values predicted by our model and the experimental value, was calculated from the objective function, OF, according to the formula

$$\mathrm{RMSE} = \sqrt{\frac{\mathrm{OF}}{n}} \tag{15}$$

Table 1 also shows the RMSE for the PR predictions when constant values of the binary interaction parameters were used. The last column in Table 1 entitled 'RMSE of const. $k_{12}$' lists the RMSE resulting from comparing the predictions of PR equation of state used with a constant-$k_{12}$ mixing rule with the experimental data. The systems tested can be divided into three categories as shown in Table 2. The improvements obtained through the use of the developed formula are clear for the systems listed in the first two columns. When the two components in the systems differ substantially in terms of their size or polarity, the use of a cubic equation of state like Peng–Robinson with the classical mixing rule is usually not preferred. However, with the use of the developed formula, the use of PR and vdW mixing rule can be extended to systems in the first and second columns of Table 2 with significantly improved results.

The lumping of components into categories can lend itself to an easier usage of the developed formula. Regression analysis was performed on different categories of components and the obtained parameters are shown in Table 3, which shows the systems for which the RMSE value was less than 10%. For systems that belong to other categories such as hydrogen sulfide/light alkanes or nitrogen/light alkanes, it is better to use the adjustable parameters obtained for individual pairs as they will produce better results.

### *Comparison with constant-$k_{ij}$ predictions*

The use of the developed formula considerably improved the prediction of the PR/vdW model for the systems shown in the first column of Table 2. Figs. 1 and 2 show this improvement graphically. Fig. 1 shows the Pxy vapor–liquid equilibrium diagram for ethane and hydrogen sulfide at 255 and 283 K using the semi-empirical correlation for $k_{ij}$ as compared with the results of the constant-$k$ calculations and with the experimental data. Fig. 2 shows the Pxy equilibrium diagram for methane and toluene at 313 K using the semi-empirical correlation for $k_{ij}$ as compared with the results of the constant-$k$ calculations and with the experimental data.

The improvement in the prediction can also be seen with the systems in the second column of Table 2. Fig. 3 shows the Pxy vapor–liquid equilibrium diagram for nitrogen and ethane at 172 and 220 K using the semi-empirical correlation for $k_{ij}$ as compared with the results of the constant-$k$ calculations and with the experimental data. On the other hand, the improvement in the prediction for systems in the third column is small yet significant as shown in Fig. 4, which shows the Pxy vapor–liquid equilibrium diagram for methane and carbon dioxide at 250 and 270 K using the semi-empirical correlation

for $k_{ij}$ as compared with the results of the constant-$k$ calculations and with the experimental data.

*Extension to ternary systems*

The developed formula was used to predict the vapor–liquid equilibrium for ternary systems and compared with experimental data reported in the literature. For meaningful comparisons, the developed model was used to obtain the liquid and vapor composition at equilibrium at a given temperature, pressure and liquid composition of component 1, which is the most volatile component. The experimental and predicted points can then be presented on one ternary diagram. The experimental data in this comparison were not used during regression.

Fig. 5 shows the ternary liquid vapor equilibrium diagram for methane, carbon dioxide and propane at 270 K and 55 bar using the semi-empirical correlation for $k_{ij}$ as compared with the results of the constant-$k$ calculations and with the experimental data published be Webster and Kidnay [54]. The predictions of the two models are similar for this system, but this was not always the case. In the system nitrogen–ethane–carbon dioxide, both models failed to provide satisfactory predictions of the experimental data. Fig. 6 shows the ternary liquid vapor equilibrium diagram for nitrogen, carbon dioxide and ethane at 270 K and 60 bar using the semi-empirical correlation for $k_{ij}$ as compared with the results of the constant-$k_{ij}$ calculations and with the experimental data published by Brown et al. [55]. For this system, both model predictions were not close to the experimental data but their predictions were different from one another. Performing the comparison on the same system at different conditions also showed that both models were unable to predict satisfactorily the experimental results. The constant-$k_{ij}$ model did not predict the existence of the two phases within a subset of composition range as compared with the formula developed in this work, which predicted a continuous two-phase region similar to the experimental behavior at 220 K and 8 bar. However, quantitative agreement was not obtained as shown in Fig. 7.

## Conclusions

This work showed that the complexity of a mixing rule can be incorporated into a semi-empirical correlation for the binary interaction parameter for the classical van der Waals mixing rules. The adjustable parameters were obtained for use with the developed formula. The formula predictions were universally better than the constant-$k$ approach when applied to binary systems of hydrocarbons and related compound. Values for the adjustable parameters were also obtained for categories of similar components, which would allow the extension of this work to systems for which no experimental data are available. The application of the developed formula on ternary systems did not show significant improvements over the constant-$k_{ij}$ approach.

## References

[1] Chen CC, Mathias PM. Applied thermodynamics for process modeling. AIChE J 2002;48(2):194–200.
[2] Peng DY, Robinson DB. A new two-constant equation of state. Ind Eng Chem Fundam 1976;15(1):59–64.
[3] Huron MJ, Vidal J. New mixing rules in simple equations of state for representing vapour–liquid equilibria of strongly non-ideal mixtures. Fluid Phase Equilib 1979;3(4):255–71.
[4] Wong DSH, Sandler SI. A theoretically correct mixing rule for cubic equations of state. AIChE J 1992;38(5):671–80.
[5] Orbey H, Sandler SI. Modeling vapor–liquid equilibria: cubic equations of state and their mixing rules. Cambridge Univ. Press; 1998.
[6] Soave G, Gamba S. SRK equation of state: predicting binary interaction parameters of hydrocarbons and related compounds. Fluid Phase Equilib 2010.
[7] Hildebrand JH, Prausnitz J, Scott RL. Regular and related solutions: the solubility of gases, liquids, and solids. New York: Van Nostrand Reinhold Co.; 1970.
[8] Ohgaki K, Katayama T. Isothermal vapor–liquid equilibrium data for the ethane–carbon dioxide system at high pressures. Fluid Phase Equilib 1977;1(1):27–32.
[9] Brown TS, Kidnay AJ, Sloan ED. Vapor–liquid equilibria in the carbon dioxide–ethane system. Fluid Phase Equilib 1988;40(1–2):169–84.
[10] Leu AD, Robinson DB. Equilibrium phase properties of the n-butane carbon dioxide and i-butane carbon dioxide binary systems. J Chem Eng Data 1987;32(4):444–7.
[11] Weber LA. Simple apparatus for vapor liquid equilibrium measurements with data for the binary systems of carbon dioxide with n-butane and i-butane. J Chem Eng Data 1989;34(2):171–5.
[12] Leu AD, Robinson DB. Equilibrium phase propertied of selected carbon-dioxide binary-systems normal pentane carbon dioxide and isopentane carbon dioxide. J Chem Eng Data 1987;32(4):447–50.
[13] Besserer GJ, Robinson DB. Equilibrium phase properties of i-pentane carbon dioxide system. J Chem Eng Data 1975;20(1):93–6.
[14] Sebastian HM, Simnick JJ, Lin H-M, Chao K-C. Gas–liquid equilibrium in mixtures of carbon dioxide + toluene and carbon dioxide + m-xylene. J Chem Eng Data 1980;25(3):246–8.
[15] Pozo de Fernandez ME, Zollweg JA, Streett WB. Vapor–liquid equilibrium in the binary system carbon dioxide + n-butane. J Chem Eng Data 1989;34(3):324–8.
[16] Hsu JJC, Nagarajan N, Robinson RL. Equilibrium phase compositions, phase densities, and interfacial tensions for $CO_2$ + hydrocarbon systems. 1. $CO_2$ + n-butane. J Chem Eng Data 1985;30(4):485–91.
[17] Kalra H, Krishnan TR, Robinson DB. Equilibrium phase properties of carbon dioxide n-butane and nitrogen hydrogen sulfide systems at sub-ambient temperatures. J Chem Eng Data 1976;21(2):222–5.
[18] Li Y-H, Dillard KH, Robinson RL. Vapor–liquid phase equilibrium for carbon dioxide-n-hexane at 40, 80, and 120 degree C. J Chem Eng Data 1981;26(1):53–5.
[19] Wagner Z, Wichterle I. High-pressure vapour–liquid equilibrium in systems containing carbon dioxide, 1-hexene, and n-hexane. Fluid Phase Equilib 1987;33(1–2):109–23.
[20] Tochigi K, Hasegawa K, Asano N, Kojima K. Vapor–liquid equilibria for the carbon dioxide + pentane and carbon dioxide + toluene systems. J Chem Eng Data 1998;43(6):954–6.
[21] Cheng HZ, Defernandez MEP, Zollweg JA, Streett WB. Vapor liquid equilibrium in the system carbon dioxide + n-pentane from 252 K to 458 K at pressures to 10 MPa. J Chem Eng Data 1989;34(3):319–23.
[22] Weng WL, Lee MJ. Vapor–liquid equilibrium of the octane/carbon dioxide, octane/ethane, and octane/ethylene systems. J Chem Eng Data 1992;37(2):213–5.
[23] Kim JH, Kim MS. Vapor–liquid equilibria for the carbon dioxide + propane system over a temperature range from 253.15 to 323.15 K. Fluid Phase Equilib 2005;238(1):13–9.

[24] Hamam SEM, Lu BCY. Isothermal vapor–liquid equilibriums in binary system propane–carbon dioxide. J Chem Eng Data 1976;21(2):200–4.
[25] Niesen VG, Rainwater JC. Critical locus, (vapor + liquid) equilibria, and coexisting densities of (carbon dioxide + propane) at temperatures from 311 K to 361 K. J Chem Thermodyn 1990;22(8):777–95.
[26] Ohgaki K, Sano F, Katayama T. Isothermal vapor–liquid equilibrium for binary systems containing ethane at high pressures. J Chem Eng Data 1976;21(1):55–8.
[27] Lhotak V, Wichterle I. Vapor–liquid equilibria in the ethane n-butane system at high pressures. Fluid Phase Equilib 1981;6(3–4):229–35.
[28] Blanc CJ, Setier JCB. Vapor liquid equilibria for the ethane propane system at low temperature. J Chem Eng Data 1988;33(2):111–5.
[29] Uchytil P, Wichterle I. Liquid vapor critical region of the most volatile component of a ternary-system. 1. Vapor–liquid equilibria in the ethane–propane–n-butane system. Fluid Phase Equilib 1983;15(2):209–17.
[30] Li IPC, Wong Y-W, Chang S-D, Lu BCY. Vapor–liquid equilibriums in systems n-hexane–benzene and n-pentane–toluene. J Chem Eng Data 1972;17(4):492–8.
[31] Laugier S, Richon D. Vapor–liquid equilibria for hydrogen sulfide + hexane, + cyclohexane, + benzene, + pentadecane, and + (hexane + pentadecane). J Chem Eng Data 1995;40(1):153–9.
[32] Leu AD, Robinson DB. Equilibrium phase properties of the n-butane–hydrogen sulfide and isobutane–hydrogen sulfide binary systems. J Chem Eng Data 1989;34(3):315–9.
[33] Théveneau P, Coquelet C, Richon D. Vapour–liquid equilibrium data for the hydrogen sulphide + n-heptane system at temperatures from 293.25 to 373.22 K and pressures up to about 6.9 MPa. Fluid Phase Equilib 2006;249(1–2):179–86.
[34] Ng HJ, Kalra H, Robinson DB, Kubota H. Equilibrium phase properties of the toluene–hydrogen sulfide and heptane–hydrogen sulfide binary systems. J Chem Eng Data 1980;25(1):51–5.
[35] Huang SSS, Robinson DB. Vapor–liquid equilibrium in selected aromatic binary systems: m-xylene–hydrogen sulfide and mesitylene–hydrogen sulfide. Fluid Phase Equilib 1984;17(3):373–82.
[36] Mraw SC, Hwang S-C, Kobayashi R. Vapor–liquid equilibrium of the methane–carbon dioxide system at low temperatures. J Chem Eng Data 1978;23(2):135–9.
[37] Wichterle I, Kobayashi R. Vapor–liquid equilibrium of methane–ethane system at low temperatures and high pressures. J Chem Eng Data 1972;17(1):9–12.
[38] Janisch J, Raabe G, Köhler J. Vapor−liquid equilibria and saturated liquid densities in binary mixtures of nitrogen, methane, and ethane and their correlation using the VTPR and PSRK GCEOS. J Chem Eng Data 2007;52(5):1897–903.
[39] Miller RC, Kidnay AJ, Hiza MJ. Liquid + vapor equilibria in methane + ethene and in methane + ethane from 150.00 to 190.00 K. J Chem Thermodyn 1977;9(2):167–78.
[40] Lin Y-N, Chen RJJ, Chappelear PS, Kobayashi R. Vapor–liquid equilibrium of the methane–n-hexane system at low temperature. J Chem Eng Data 1977;22(4):402–8.
[41] Olds RH, Sage BH, Lacey WN. Methane–isobutane system. Ind Eng Chem 1942;34:1008–13.
[42] Reiff WE, Peters-Gerth P, Lucas K. A static equilibrium apparatus for (vapour + liquid) equilibrium measurements at high temperatures and pressures. Results for (methane + n-pentane). J Chem Thermodyn 1987;19(5):467–77.
[43] Kahre LC. Low-temperature K data for methane n-pentane. J Chem Eng Data 1975;20(4):363–7.
[44] Brown TS, Niesen VG, Sloan ED, Kidnay AJ. Vapor–liquid equilibria for the binary systems of nitrogen, carbon dioxide, and n-butane at temperatures from 220 to 344 K. Fluid Phase Equilib 1989;53:7–14.
[45] Shibata SK, Sandler SI. High-pressure vapor–liquid equilibria involving mixtures of nitrogen, carbon dioxide, and n-butane. J Chem Eng Data 1989;34(3):291–8.
[46] Brown I, Ewald A. Liquid–vapour equilibria. II. The system benzene–n-heptane. Aust J Chem 1951;4(2):198–212.
[47] Ohgaki K, Katayama T. Isothermal vapor–liquid equilibrium data for binary systems containing carbon dioxide at high pressures: methanol-carbon dioxide, n-hexane–carbon dioxide, and benzene–carbon dioxide systems. J Chem Eng Data 1976;21(1):53–5.
[48] Jiménez-Gallegos R, Galicia-Luna LA, Elizalde-Solis O. Experimental vapor–liquid equilibria for the carbon dioxide + octane and carbon dioxide + decane systems. J Chem Eng Data 2006;51(5):1624–8.
[49] Nagarajan N, Robinson RL. Equilibrium phase compositions, phase densities, and interfactial tensions for $CO_2$ + hydrocarbon systems.2. $CO_2$ + n-decane. J Chem Eng Data 1986;31(2):168–71.
[50] Sebastian HM, Simnick JJ, Lin HM, Chao KC. Vapor–liquid equilibrium in binary mixtures of carbon dioxide + n-decane and carbon dioxide + n-hexadecane. J Chem Eng Data 1980;25(2):138–40.
[51] Wei MSW, Brown TS, Kidnay AJ, Sloan ED. Vapor + liquid equilibria for the ternary system methane + ethane + carbon dioxide at 230 K and its constituent binaries at temperatures from 207 to 270 K. J Chem Eng Data 1995;40(4):726–31.
[52] Broyden CG. A class of methods for solving nonlinear simultaneous equations. Math Comp 1965;19(92):577–93.
[53] Michelsen ML. The isothermal flash problem. Part 1. Stability. Fluid Phase Equilib 1982;9:1–19.
[54] Webster LA, Kidnay AJ. Vapor−liquid equilibria for the methane−propane−carbon dioxide systems at 230 K and 270 K. J Chem Eng Data 2001;46(3):759–64.
[55] Brown TS, Sloan ED, Kidnay AJ. Vapor–liquid equilibria in the nitrogen + carbon dioxide + ethane system. Fluid Phase Equilib 1989;51:299–313.
[56] Kalra H, Robinson DB, Krishnan TR. The equilibrium phase properties of the ethane–hydrogen sulfide system at subambient temperatures. J Chem Eng Data 1977;22(1):85–8.
[57] Legret D, Richon D, Renon H. Vapor–liquid equilibrium of methane–benzene, methane–methylbenzene (toluene), methane–1,3-dimethylbenzene (m-xylene), and methane–1,3,5-trimethylbenzene (mesitylene) at 313.2 K up to the critical point. J Chem Eng Data 1982;27(2):165–9.
[58] Davalos J, Anderson WR, Phelps RE, Kidnay AJ. Liquid-vapor equilibria at 250.00 deg.K for systems containing methane, ethane, and carbon dioxide. J Chem Eng Data 1976;21(1):81–4.